Direct Drive Wave Energy Array with Offshore Energy Storage Supplying Off-Grid Residential Load

Direct Drive Wave Energy Array with Offshore Energy Storage Supplying Off-Grid Residential Load

Marios Charilaos Sousounis [1*], Leong Kit Gan [1], Aristides E. Kiprakis [1] and Jonathan K.H. Shek [1]

[1]*Institute for Energy Systems, School of Engineering, The University of Edinburgh, The King's Buildings, Mayfield Road, Edinburgh, EH9 3DW, United Kingdom*

[*]*Email: M.Sousounis@ed.ac.uk*

Keywords: Energy storage, wave energy converter, wave array, point absorber, supercapacitors.

Abstract

Current developments in wave energy conversion has focussed on locations where the wave energy resource is highest; using large devices to generate hundreds of kilowatts of power. However, it is possible to generate power from low power waves using smaller wave energy devices. These lower rated wave energy converters can form arrays to supply power to remote coastal or island communities which are off-grid. The paper introduces wave-to-wire modelling of wave energy arrays for off-grid systems using low power permanent magnet linear generators. Offshore energy storage at the DC link is added to keep the voltage constant along with a current controller for the inverter in order to supply constant low harmonic power to the residential load connected off-grid. Simulation results produced in MATLAB/Simulink environment show that the wave energy array can generate power independently from the residential side by keeping the system stable using offshore storage. In addition, two different types of controllers for wave energy devices that use permanent magnet linear generators are compared based on the power captured from the waves.

1 Introduction

Island communities and rural coastal areas are often isolated from the electricity network. For such areas the energy supply comes from autonomous diesel or oil fired generators. The utilisation of wave energy converters (WECs) for island communities and remote coastal areas can increase the reliability of supply and decrease the fuel cost needed for fossil fuel generators. Moreover, when the area is connected to the main electrical network the WECs can contribute to the overall renewable energy production. However, due to the variability of the resource, the energy WECs produce cannot be directly used at domestic level [1]. Power smoothing and quality improvement is needed. Researchers in [2] place the energy storage element onshore, on the AC side, so that the energy exported at the point of common connection meets the power quality requirements. Another research presented in [3] proposes a hybrid storage system at the DC link for power smoothing. However, the power exported in [3] is highly variable. In reference [4] authors use supercapacitor storage technology at the DC link in order to smooth the power fluctuations of the power generated for a single WEC. The effectiveness of the storage technology at the DC link is demonstrated though the wave energy system does not export power to the grid. In this research paper, two design changes have been considered in order to increase the power quality output of the WEC array. Firstly, the energy storage is installed at the common DC link using a bidirectional Ćuk converter. Secondly, a current controller is implemented for the inverter to supply constant active power at the residential load.

The wave energy resource [5] is significant and can contribute to the demand for renewable electricity. However, a large amount of the wave energy resource can be characterised as “low” and can be found in many areas around the world such as the Chinese coastline and the Mediterranean Sea [4, 6]. One of the key aspects of this paper is to investigate the application of a low power WEC array to supply power to an off-grid residential load.

At present, a number of different designs exist that convert wave energy to electrical power. These designs usually have power take-off systems that use conventional high speed rotating electrical generators such as induction and synchronous machines [4, 7, 8]. In [4] authors use a permanent magnet generator with ball-screw to convert the linear motion of the point absorber to rotating speed for the generator. On the other hand, authors in [8] use a hydraulic motor system with hydraulic energy storage to drive an induction generator. For WECs that are based on the point absorber concept it is suggested

that a direct drive power take-off system that uses permanent magnet linear generators (PMLG) can be a viable alternative; the first-generation Archimedes Wave Swing being one of the better known examples [9, 10]. By using PMLGs for WECs the complex mechanical interface between the prime mover and the rotor is eliminated and the conversion losses are reduced. In addition, in a Vernier hybrid machine operation speeds are low as dictated by the incoming waves and the construction of the machine is not as complicated as other traverse flux permanent magnet machines. However, cost and complexity of PMLG are higher than conventional machines and, in addition, special design needs to be introduced in order to avoid high eddy-current losses [11, 12].

Another key aspect of supplying quality power to residential loads is the control method used to control the PMLGs. Controlling PMLGs for wave energy extraction is not as straightforward as wind energy extraction. The irregular motion of the sea complicates the control structure and the measurements required to achieve maximum energy extraction in a broad scale of sea conditions. Numerous control methods for different types of machines have been developed through the years. A comprehensive study of these methods is given in [13]. For the control of the specific PMLG authors in [10] and [14] explain the background and give examples of sub-optimal and optimal control giving examples of the advantages and disadvantages in each case.

The aim of this research paper is to propose a wave-to-wire system model of a complete wave energy conversion array for off-grid operation which integrates offshore energy storage. Offshore energy storage at the DC link of this system is the key aspect of this study due to the fact that it keeps both sides of the system, residential side and generator side, in stability. In section 2 the methodology of the research is given by defining all the different parts of the model. These include the wave resource, the generator and its controller, the common DC link for the array, energy transmission to shore and the residential side. In depth details are given for the design of the offshore storage element and the control side of the PMLG. In section 3 the overall operation of the system is described under different operating conditions. Firstly, the generator control options are compared and power exported from the offshore system to the residential side is assessed. Afterwards, power demand, voltage variations and power quality are described based on their suitability for residential use. Conclusions are summarised in the final section of this paper.

2 System description

This section describes the wave-to-wire system model developed in MATLAB/Simulink. The block diagram of the proposed electrical configuration of the WEC array for off-grid operation with offshore energy storage is shown in Figure 1.

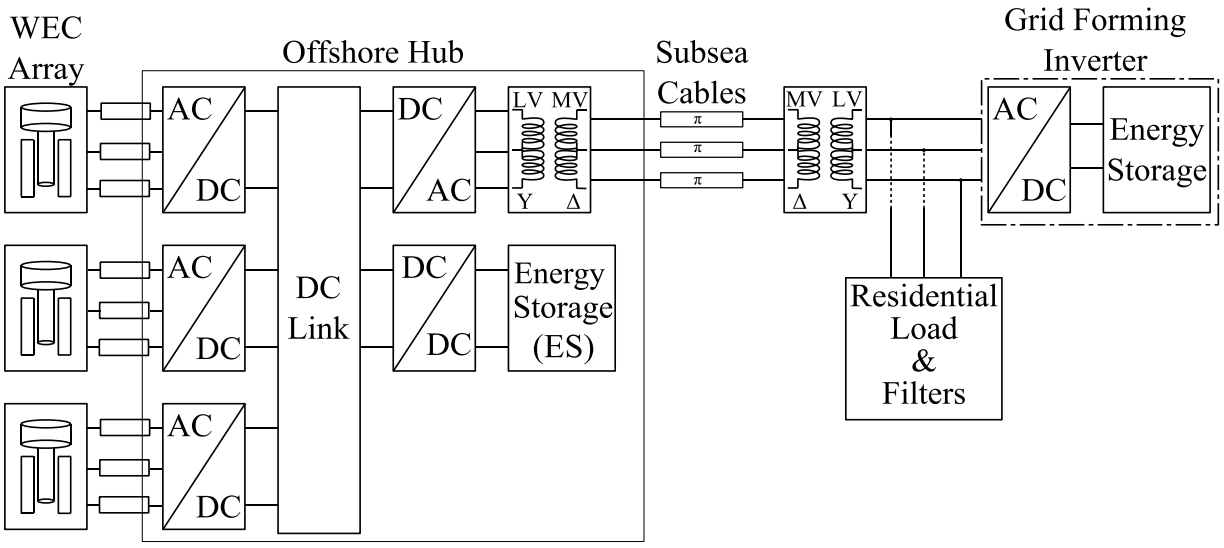

Figure 1. Block diagram of the wave-to-wire model developed in MATLAB/Simulink

The WEC array developed is composed of three WECs. Each WEC has short three-phase cables to the offshore hub and it is directly connected to an active rectifier. Active rectifiers are controlled independently and convert AC current to DC. The DC outputs from all the active rectifiers are then connected to a common DC link. In order to keep the DC link voltage constant, energy storage is included in the offshore hub. A DC/DC Ćuk converter is utilised to step-up the voltage of the supercapacitors to the DC link voltage level. The DC/AC inverter is controlled so that a specific amount of power is transferred to shore based on the average power produced by the WEC array. In order to transfer power from the offshore hub to the shore, medium voltage AC transmission is implemented using transformers. On the shore the grid forming inverter acts as a grid, keeping the voltage constant and providing active and reactive power to the residential load if needed. For the purposes of this research the energy storage of the grid forming inverter is supposed to be able to provide autonomy to

the system for a long period of time. A similar electrical design using an underwater hub for the wave energy array is described in [15].

2.1 The wave resource

As input to the model, an irregular one-dimensional waveform of the wave height is used with 0.1*s* sampling time. The wave height was generated using a Pierson-Moskowitz spectrum. The same wave input is used for all three devices considered in the simulation but in each device the waveform is shifted slightly to show that the devices are placed near to each other. The wave height and the wave spectral density of the wave input is shown in Figure 2.

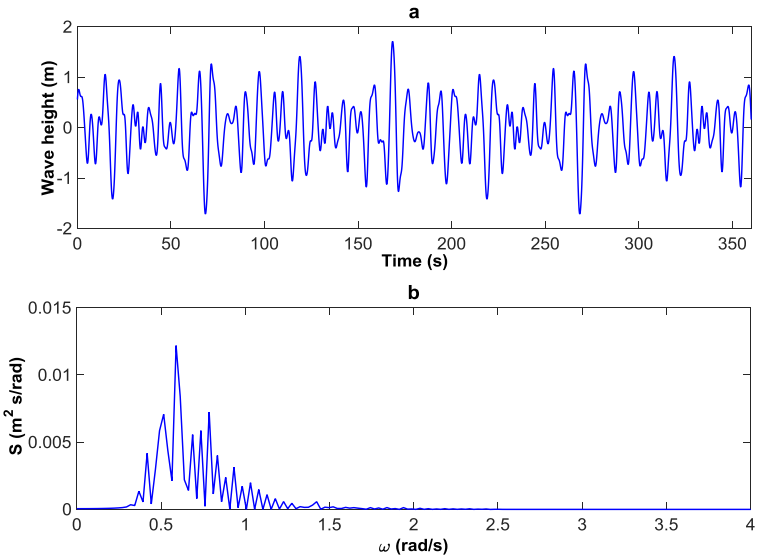

Figure 2. The wave resource **a.** Time series of the wave height **b.** wave spectral density of the time series

As it is shown in Figure 2a the maximum wave height is less than 2*m* and based on Figure 2b the frequency with the higher energy density is around 0.6 rad/s which leads to a period of around 10.5*s*. Based on the above we can characterise the wave energy resource as low energy resource. In addition, as it is shown in Figure 2b the frequencies of the wave resource vary from 0.368 *rad/s* to 1.424 *rad/s* which leads to periods between 4.41*s* and 17.7*s* and therefore the spectrum of the wave input can be defined as narrow banded. The wave input described above applies a force to the point absorber and consequently to the translator of the PMLG. The operation and modelling of the PMLG is described below.

2.2 The point absorber and electrical generator

The point absorber model in this paper is represented using a mass spring damper system as shown in Figure 3a. The point absorber parameters are given in Table 1 and the equation of motion in (1). It is assumed that the point absorber is moving only at the heave direction with one degree of freedom and that the damping is linear. As it is shown in Figure 3b and (2) the hydrodynamic parameters of the point absorber are also considered by using added mass, A_m, and added damping, A_d. The hydrodynamic parameters are calculated based on linear hydrodynamic theory using already calculated values. By knowing the frequencies of the irregular wave input the hydrodynamic parameters of the system change during operation [14]. The point absorber model used in this research is a simplified model as the main focus is on the electrical side of the WEC arrays.

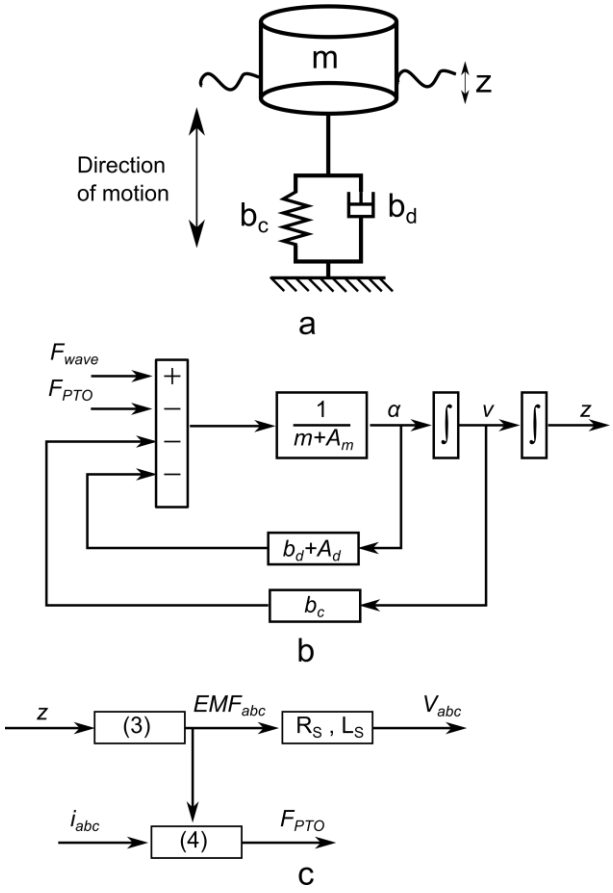

Figure 3. **a**. Block diagram of the mass spring damper representing the point absorber. **b**. Block diagram of the hydrodynamic model and power take-off system. **c**. Block diagram of the electrical part of the PMLG.

$$ma + b_d v + b_c z = F_{wave} \quad (1)$$

$$(m + A_m)a + (b_d + A_d)v + b_c z + F_{PTO} = F_{wave} \quad (2)$$

Where m is the mass, b_d is the damping coefficient, b_c is the spring stiffness, a the acceleration, v the velocity, z the displacement of the point absorber, F_{wave} is the excitation force by the waves and F_{PTO} is the force applied by the power take-off (PTO). The *EMF* of the generator and the F_{PTO} can be calculated using equations (3) and (4) [16].

$$\begin{cases} EMF_a = -N_t \frac{\pi}{\tau_p} \Phi \sin\left(\frac{\pi}{\tau_p} z\right) \frac{dz}{dt} \\ EMF_b = -N_t \frac{\pi}{\tau_p} \Phi \sin\left(\frac{\pi}{\tau_p} z - \frac{2\pi}{3}\right) \frac{dz}{dt} \\ EMF_c = -N_t \frac{\pi}{\tau_p} \Phi \sin\left(\frac{\pi}{\tau_p} z - \frac{4\pi}{3}\right) \frac{dz}{dt} \end{cases} \quad (3)$$

$$F_{PTO} = \frac{3}{2} \frac{\pi}{\tau_p} \Phi N_t I \cos\varphi \quad (4)$$

Where N_t is the number of turns around a tooth, Φ is the flux in the tooth, I is the peak current and τ_p is the pole pitch. The current leads the EMF voltage with an angle φ. The generation of the three-phase currents is a function of displacement and is given in (5).

$$\begin{cases} i_a = -I \sin\left(\frac{\pi}{\tau_p} z + \varphi\right) \\ i_b = -I \sin\left(\frac{\pi}{\tau_p} z - \frac{2\pi}{3} + \varphi\right) \\ i_c = -I \sin\left(\frac{\pi}{\tau_p} z - \frac{4\pi}{3} + \varphi\right) \end{cases} \quad (5)$$

Figure 3c presents the electrical part of the PMLG modelled. The input of the electrical part is the displacement z from the power take-off model shown in Figure 3b. The three-phase EMF is generated using (3) and is converted to generator voltage using stator resistance and inductance. Table 1 presents the parameters of the buoy and Table 2 the parameters of the PMLG. The electrical part of the model also generates the F_{PTO} which is fed back to the power take-off system using (4). More details regarding the design and modelling of the PMLG can be found in [14] and [17].

Table 1: Point absorber parameters.

Symbol	Quantity	Value
m	Mass	10000 kg
A_m	Added mass at natural frequency	7936 kg
b_d	Damping	4000 Ns/m
A_d	Added damping at natural frequency	333 Ns/m
b_c	Stiffness (b_d)	31580 N/m
w_n	Absorber natural frequency	1.7771 rad/s
B_r	Buoy radius	1.5 m
B_h	Buoy height	2.75 m

Table 2: Generator parameters.

Symbol	Quantity	Value
P_{peak}	WEC peak rating	40 kW
N_t	Number of turns around a tooth	250
τ_p	Pole pitch	0.1 m
Φ	Flux in the tooth	0.1073 Wb
R_s	Stator resistance	2.9667 Ω
L_s	Stator inductance	0.0789 H

2.3 The generator controller

The generator side controller has one main objective, to maximise energy captured from the incoming waves. In order to achieve this, complex conjugate control is required; this controls F_{PTO} so that it matches the intrinsic impedance of the system. This process is described in detail in [13] and [14]. However, due to the complicated motion of the point absorber there is a need to calculate a number

of parameters in order to estimate the desired value of F_{PTO}. The process of measuring all the appropriate variables in actual systems is costly and sometimes inaccurate. For this reason researchers in [17, 18] have developed a sub-optimum controller in order to reduce complexity. In this research paper, two different types of generator controllers are tested in terms of power production, effect on the offshore storage element and complexity of implementation. The controllers compared are the sub-optimum controller and the speed controller. The speed controller which is presented in this section is a novelty of the current paper.

The principle of operation of the speed controller is based on equations (6) and (7).

$$v^{opt}(\omega) = F_{wave}(\omega)/\big(2R_i(\omega)\big) \quad (6)$$

$$P_{mec} = F_{wave} \times v \quad (7)$$

Equation (6) is described in [13] and relates desired velocity profile, v^{opt}, with the real part of intrinsic impedance of the system, R_i. In addition, for maximum power production the velocity of the translator of the PMLG must be in phase with the wave force as described in (7). Therefore using (6) and (7) we can determine the waveform of the ideal speed that the translator of the PMLG must obtain. In this research paper it is assumed that the wave height and the excitation force by the waves, F_{wave}, have a linear relationship and that the R_i is estimated based on the peak frequency of F_{wave}. This leads to an optimum velocity profile that is similar to the wave height presented in Figure 2a which can be measured in real-time operation. The calculated v^{opt} is compared to the actual velocity of the PMLG translator. The error between optimal and actual velocity, v_{error}, is fed to a *Proportional-Integral* (*PI*) controller to generate a reference PTO force signal, F_{PTO}*. In order to control the speed of the translator of the PMLG the zero *d-axis* control method used in permanent magnet synchronous machines is implemented [19]. The block diagram of the control method is shown in Figure 4a and results from the operation of the controller are given in Figure 4b.

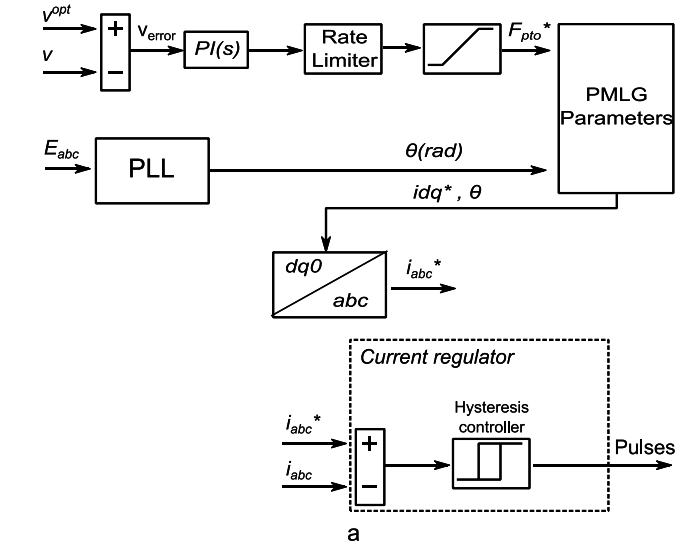

a

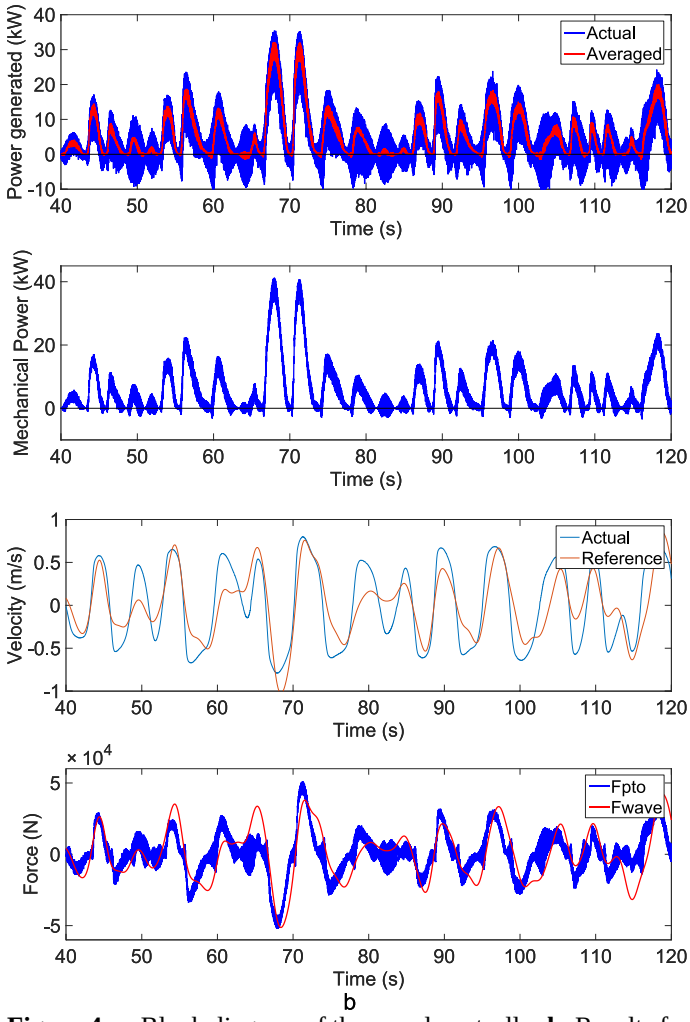

b

Figure 4. **a**. Block diagram of the speed controller **b**. Results from electrical power generated, mechanical power, velocity and force from the PMLG

It is observed that using the speed control method electrical power is absorbed by the PMLG at some instances so that the translator achieves the desired velocity. The absorbed electrical power is transferred to the mechanical part of the PMLG through the F_{PTO}. When F_{PTO} and the actual translator velocity have opposite signs the mechanical power of the PMLG is negative. The negative mechanical power in Figure 4b denotes the power supplied by the generator side converter to accelerate or decelerate the translator of the PMLG in order to match the desired velocity. This is similar to the operation of the complex conjugate control [14]. Taking a closer look at the velocity graph it is obvious that the actual speed and the reference speed do not match. This is due to a number of reasons. Firstly, the mass and the mechanical damping of the system make the system response slow. Secondly, limitations have been applied to the controller so that the system does not operate above safety limits. These limitations include acceleration, deceleration and maximum velocity restrictions for the translator of the PMLG.

2.4 DC link and energy storage

At the DC link all the power from the WEC array is collected. In Table 3 the DC link parameters are given. In addition, at the DC link the supercapacitors are connected using a DC/DC Ćuk converter to step-up the voltage from the supercapacitor voltage of $130V$ to the DC link voltage of $800V$. The DC/DC Ćuk converter ratio of 6.16 is high which decreases its performance. A lower ratio will be achieved when a larger number of WEC devices are connected at the same DC link. The additional WEC devices connected to the same DC link would require more supercapacitors, increasing the supercapacitor voltage and therefore decreasing the ratio.

2.4.1 Modelling the DC/DC Ćuk Converter: The bidirectional DC/DC Ćuk converter can be implemented by cascading the boost converter and the buck converter. It is composed from an input inductor *L1*, an energy transfer capacitor *C1*, a filter inductor *L2*, a filter capacitor *C2* and two switching devices as shown in Figure 5a. The utilisation of a bidirectional DC/DC Ćuk converter with a battery system is described in [20]. The control system of the bidirectional DC/DC Ćuk converter implemented in this study is based on the voltage-mode control. At this mode the controller tries to keep the voltage at a reference value. The error between the reference voltage and actual voltage is used as input to a

PID controller in order to construct a control voltage signal. The voltage control signal is then utilised to generate high frequency PWM signals for the switching devices *S1* and *S2*.

2.4.2 Offshore energy storage: The purpose of the offshore energy storage is twofold:

Firstly, it is responsible for keeping the DC link voltage constant at 800*V*. This is achieved by using the Ćuk converter that steps up the voltage of the supercapacitors from 130*V* to 800*V* and allows bi-directional power flow between the capacitors and the DC link. Since the WEC array delivers variable power to the DC link, the capacitors have to be able to absorb the fluctuating excess power that is not delivered to the load. The generator reaches the peak power two times within one wave period. When the combined power generated by the WEC array is higher than the power delivered by the grid side inverter the supercapacitors have to store energy. When the combined power generated by the WEC array is lower than the power delivered by the grid side inverter the supercapacitors have to release energy. Figure 5b describes this process for a single device when the power output of the WEC device is ideal and the power delivered by the inverter is constant.

Secondly, the supercapacitors will supply the WEC array any amount of active or reactive power required by the reactive power controller. As previously stated, in order to perform reactive power control and extract the maximum amount of power from the waves, the controlled WEC has to absorb power from the DC link at some instances. For this reason the negative electrical power feeding the PMLG, as described in section 2.3, must be taken into account when sizing the supercapacitor.

In order to calculate the energy storage required a worst-case scenario will be assumed. In this case it is assumed that the inverter exports constant power to the load at the highest wave energy period. The period with the highest energy was calculated at 10.5*s* in section 2.1 and the power output from the PMLG operating with a speed controller at this wave period is given in Figure 5c. From [21, 22], the energy storage should be able to store ten wave periods of rated energy from the WEC array. However, as presented in the following section, a constant power output will be based on power input to the DC link and state of charge of the supercapacitors. The rate of change of the constant power exported by the inverter is set to 5 seconds as described in the following section. As depicted in Figure 5c, the average power per WEC device when operating with a speed controller at the wave period with the highest energy is 10.95kW. Allowing the capacitors to store 10 times this energy leads to 152*Wh* per

WEC device for the worst-case scenario. In a WEC array that is composed of several devices operating at different phases, the combined power input is smoother and therefore the total energy storage requirement will be smaller, but in this research paper the worst-case scenario is considered. DC link and supercapacitor parameters are given in Table 3. The supercapacitor parameters were based on commercially available supercapacitors supplied by *Maxwell Technologies* [23].

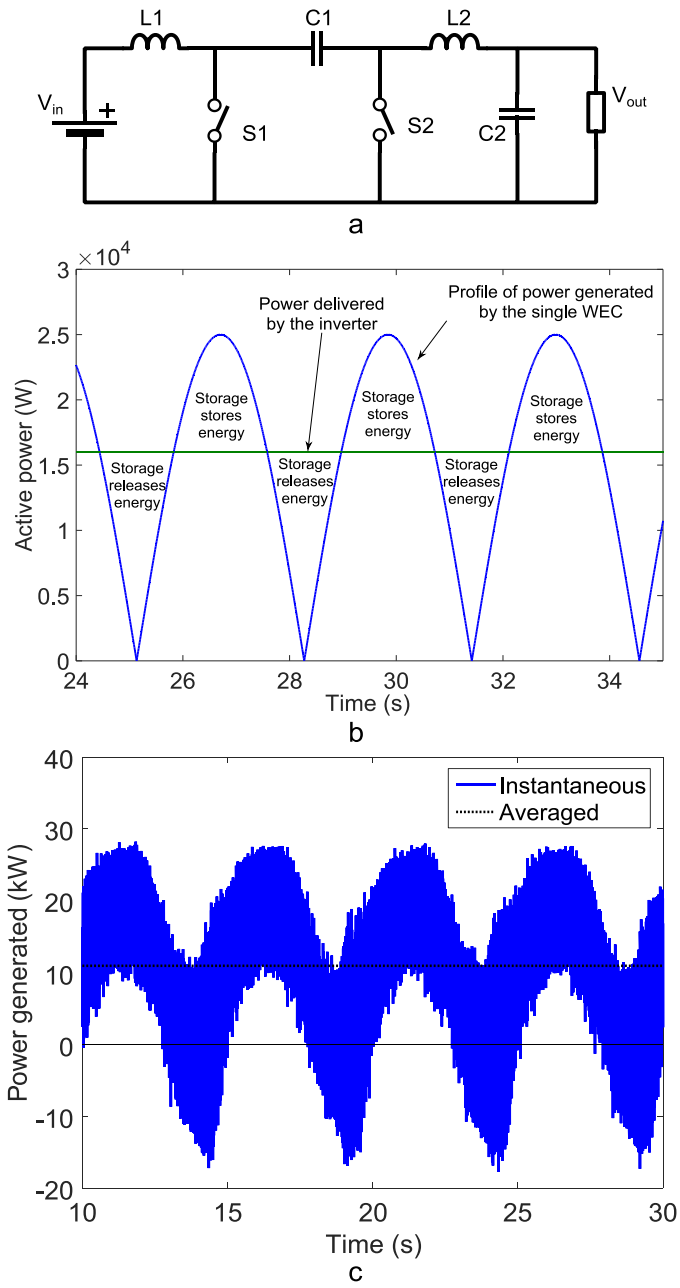

Figure 5. a Schematic diagram of the bidirectional DC/DC Ćuk converter [20]. **b**. Energy storage operation for a single WEC with ideal power generated. **c**. Calculation of the rating for the energy storage at the DC link for a single WEC device using speed control.

Table 3: DC link and energy storage parameters.

Symbol	Quantity	Value
V_{dc}	DC link voltage	800 V
V_{cap}	Supercapacitor voltage	130 V
C_{cap}	Supercapacitor capacitance	63 F
ESR_{cap}	Supercapacitor ESR	18 mΩ
E_{cap}	Supercapacitor stored energy	152 Wh
N_{cap}	Number of supercapacitors	3 (1 per WEC device)

The power delivered by the grid side inverter, shown in Figure 5b by the green constant line, is determined by the current controller which is described in section 2.5.

2.5 Grid side current controller for constant power output

The power generated by the WEC array is variable and power quality improvement is needed before it is used for domestic purposes. In [2] power quality improvement is achieved at the onshore substation with the use of a DC/DC converter and a DC/AC converter. Alternatively, in this paper power quality is achieved by both:

- The offshore energy storage at the common DC link which controls DC link voltage and was discussed in section 2.4.2.
- The current controller of the grid side inverter which controls the active and reactive power flow to the load.

The active and reactive power supplied by the inverter are defined by reference values. In this research paper the reactive power reference value is set to zero and active power reference value is set by an algorithm that takes into account the power generated by the array, the losses in the system and the

voltage level of the DC link supercapacitors. A block diagram of the current controller is shown in Figure 6 and the equations in (8) and (9).

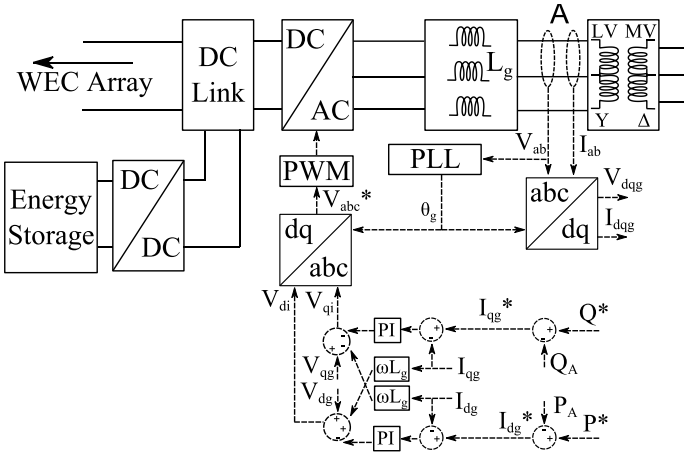

Figure 6. Block diagram of the grid side current controller. Measurements are taken from point A.

$$v_{di} = -PI(s)\left(i_{dg}^{*} - i_{dg}\right) + \omega_g L_g i_{qg} + v_{dg} \quad (8)$$

$$v_{qi} = -PI(s)\left(i_{qg}^{*} - i_{qg}\right) - \omega_g L_g i_{dg} + v_{qg} \quad (9)$$

V_{di} and V_{qi} are the reference voltages in the *dq* coordinates required by the PWM generator to generate the appropriate signals. These voltages are transformed to *abc* coordinates (V_{abc}*) using the angle θ_g calculated from point A.

The active power reference value (P*) is derived by the algorithm shown in (10):

$$P^{*} = P_{dc}^{5s} \times \eta \times \frac{V_{cap}^{meas}}{V_{cap}} \quad (10)$$

Where P_{dc}^{5s} is the average DC link power delivered by the WEC array calculated every 5 seconds, V_{cap}^{meas} is the measured voltage across the supercapacitors, V_{cap} is the rated supercapacitor voltage and η is the DC link efficiency. This algorithm ensures that if the voltage across the supercapacitors is higher than the rated voltage, more power will be delivered to the load by the inverter in order to reduce the supercapacitor voltage. If V_{cap}^{meas} drops below V_{cap}, the controller will reduce the amount of power delivered to the load. Using equation (10), it is observed that the current controller

operates independently from the state of charge of the grid forming storage element and the domestic load. This ensures that the maximum active power is delivered from the WEC array to the load and at the same time managing the stability of the DC link. Finally the voltage pulses generated by the current controller are synchronised with the grid forming inverter using a phase lock loop (PLL).

2.6 Energy transmission

Energy is transmitted to shore by using medium voltage AC cables in order to reduce transmission losses as much as possible. The voltage output from the inverter at the offshore hub is $400V$. The transformer steps-up the voltage to $13.2kV$ in order to have reduced losses in the cables. The three-phase subsea cables are modelled using the π-section. Distances from low power WEC arrays will be short and therefore 1km of distance is considered. The onshore transformer steps-down the voltage from $13.2kV$ to $400V$ for residential use. The parameters of the transformers and cables are given in Table 3.

Table 4: Transformer and cable parameters.

Parameters	*Value*
Cable length	1 *km*
Cable resistance	0.197 *Ω/km*
Cable inductance	0.742 *mH/km*
Cable capacitance	0.311 *μF/km*
Transformer rating	150 *kVA*
Wye resistance	0.025 *pu*
Wye inductance	0.083 *pu*
Delta resistance	0.005 *pu*
Delta inductance	0.026 *pu*

2.7 The residential side

The residential side is composed of three parts:

- The grid forming inverter
- The residential filter
- The residential load model

The grid forming inverter keeps the grid voltage and the frequency at a constant level. It is composed of four batteries per phase, rated at $312.5Ah$. The batteries are connected to a DC/DC boost converter to step-up the voltage and three single phase inverters to form the three-phase voltage source.

As stated above, the grid forming inverter is supposed to be able to provide power to the domestic load for a long period of time. In this paper battery storage is considered for the grid forming inverter since the load study is limited to power levels that batteries can be used. The residential filter is keeping the voltage and current total harmonic distortion (VTHD and ITHD) to approved levels despite the changes in active and reactive load demand. The residential filter is a single tuned filter with characteristic frequency, same as the switching frequency of the inverter controller, 2500*Hz*. More details about the grid-forming inverter and experimental results of this system can be found in [20].

In off-grid networks, especially where the power supply comes from a variable resource such as the sea waves, voltage may vary more widely that what is expected with grid-connected systems. In such a case the assumption of constant power demand may generate unacceptable errors, as most of electric loads are voltage-dependent. The electrical demand in the system is modelled using a polynomial 'ZIP' model [24] which can produce the short term variations of a typical UK residential load. Equations (11) and (12) give the actual active and reactive power respectively, as a factor of the nominal voltage, active and reactive powers and the instantaneous rms voltage.

$$P = P_{nom}\left[Z_p\left(\frac{V}{V_{nom}}\right)^2 + I_p\left(\frac{V}{V_{nom}}\right) + P_p\right] \quad (11)$$

$$Q = Q_{nom}\left[Z_q\left(\frac{V}{V_{nom}}\right)^2 + I_q\left(\frac{V}{V_{nom}}\right) + P_q\right] \quad (12)$$

P_{nom} and Q_{nom} are the active and reactive power demand from the household including all the appliances, V is the voltage at the load, V_{nom} is the nominal voltage at the load and Z_p, I_p, P_p, Z_q, I_q and P_q are the ZIP household model averaged coefficients including all the appliances in a typical household. Active and reactive power demand time series results are given in section 3.2.

3 System operation results

Simulation results presented in this section are based on the wave resource presented in section 2.1. In section 3.1 the power generation of the WEC array is studied and in section 3.2 the residential side is presented. As stated in section 2, power generation side is operating independently from the residential side due to offshore storage at the DC link. Simulation results to present this are depicted below.

3.1 Comparison of generator controllers

Two different generator control options, as described in section 2.3 are compared. The results are presented in Figure 7:

- Sub-optimal control. The generator does not require any power from the DC link.
- Speed controller. The controller calculates optimum velocity and tries to reduce the error between actual velocity of the translator and the optimum velocity.

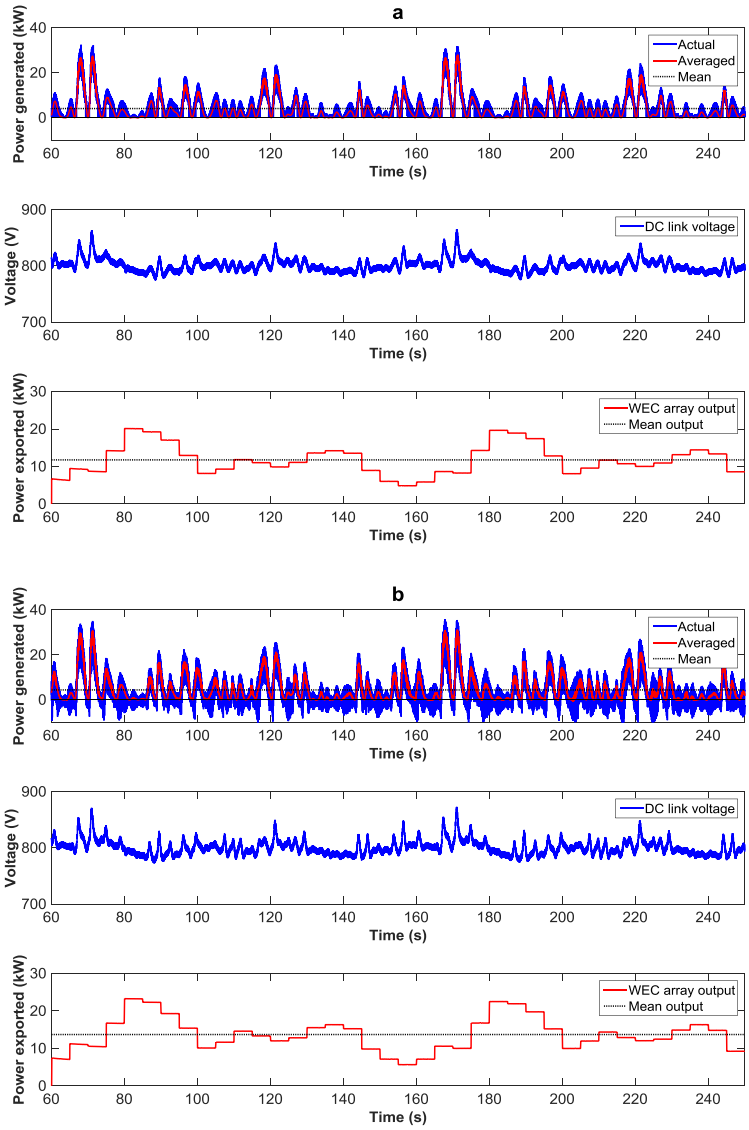

Figure 7. Results from the operation of the WEC array for **a**. sub-optimal control and **b**. speed control.

In Figure 7 power generated, power exported and DC link voltage are presented for the two different generator controller types. In terms of power generation it is observed that the mean power generated by the sub-optimal controller is 4.089kW and total energy produced is 0.216kWh over the 190 seconds period. The same results for the speed controller are 4.409kW and 0.233kWh. The speed controller generates more power compared to the sub-optimal controller. The main reason is that the speed controller drives the generator as a motor at some instances in order to synchronise the translator speed with the incoming waves. For the case of the speed controller which is presented in Figure 7b the maximum power absorbed per instance reaches 10kW and the total negative energy for the 190 seconds simulation is 0.028kWh. It must be noted that the negative energy values are included in the energy generation values given above and that the values for power generation are taken from one of the three WEC devices tested whereas power exported is based on the combine power from the WEC array.

Another important aspect which is compared in Figure 7 is the power exported from the grid side controller to the residential side. Power exported is dictated by (9) defined in section 2.5 and is directly affected by the capacitor voltage and the power generated by the WEC array. In Figure 7a the power exported by the sub-optimal controller can be seen with a mean value during the 190 seconds simulation of 11.76kW. Respectively, when the WEC array is operated by the speed controller the mean power exported is 13.71kW. As expected, based on the power generation from one WEC device discussed above, power exported from the speed controller is 14.2% higher compared to the sub-optimum controller. In addition, the power exported in all cases is always positive which means that power from the inverter is flowing towards the residential side. The fact that power is not flowing from the grid-forming inverter to the WECs increases system efficiency compared to a conventional system. The efficiencies of different parts of the system are presented in Table 5 which are calculated using equations (13) – (15). This balance of power between the generator and the power exported is achieved by using the offshore energy storage.

The aim of the offshore storage is to maintain the DC link voltage constant despite the rapid changes in power demand and generation from the WECs and the power exported from the inverter. In Figure 7 results from the DC link voltage are presented. In all cases the variation of the DC link voltage

is up to 10% which is within the advisable limits for the supercapacitor voltage. The use of supercapacitors at as the offshore energy storage allows fast charge and discharge providing good DC link voltage regulation.

$$n_{WEC}^{averaged} = \frac{generator\ output}{wave\ force \times v^{opt}(\omega)} \quad (13)$$

$$n_{DC\ link}^{averaged} = \frac{inverter\ output}{generator\ output + battery\ power\ flow} \quad (14)$$

$$n_{transmission}^{averaged} = \frac{power\ available\ at\ the\ load}{inverter\ output} \quad (15)$$

Table 5. Efficiency at different parts of the system for the sub-optimum and speed controller.

	Sub-optimum controller	*Speed controller*
WEC averaged efficiency	64.18%	69.89%
DC link efficiency	91.23%	93.39%
Transmission system efficiency	96.08%	94.53%

3.2 Residential side simulation results

Power exported from the inverter is consumed at the residential side. The residential side modelling is described in section 2.7 and simulation results of the power demanded, residential voltage and grid-forming inverter power flow are given in Figure 8. Since both generator controllers have a similar profile of power exported, only the simulation results acquired from the speed controller are considered in Figure 8.

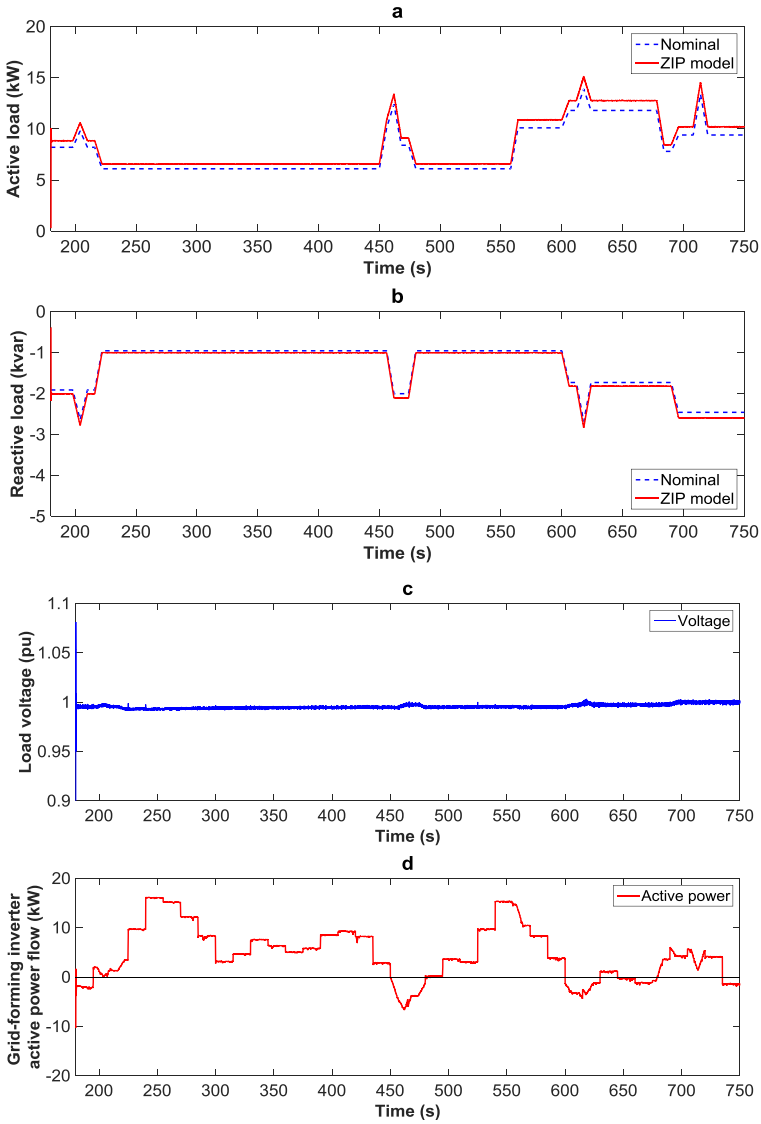

Figure 8. Residential side simulation results. **a**. Active power demand **b**. Reactive power demand **c**. Voltage at the load **d**. Active power at the grid.

Figure 8a shows the nominal and the ZIP model active power demand. The ZIP model power demand is affected by the voltage variations of the load voltage which is displayed in Figure 8c. As it can be seen the actual demand for power is higher compared to the nominal power demand of the residential loads. A similar trend appears in Figure 8b for the reactive power demand of the residential load. Reactive power is only supplied by the grid forming inverter to the residential load since the inverter controller is set to export active power only. Figure 8c displays the RMS voltage of the load in per unit (pu) and Figure 8d the power absorbed or delivered by the grid-forming inverter. For most of the simulation time the grid-forming inverter active power flow is positive (Figure 8d) which means that

the WEC array supplies active power to the residential load and the excess active power is absorbed by the grid-forming inverter. Between 450s and 500s active power flow turns negative due to the active power spike demand (Figure 8a). This means that the grid-forming inverter supplies the residential load with active power that the WEC array is unable to do so. Finally, the VTHD at the residential terminals varies between 0.28% and 2.44% which is within the limits of residential operation.

5 Conclusion

In this paper a novel wave-to-wire model of a WEC array for off-grid applications is presented. A key contribution of this research is the addition of offshore energy storage at the DC link to keep the voltage constant and provide power to the generator when needed. The inverter of the system is controlled to supply low harmonic active power to the residential load. The inverter controller ensures that the power flow is always from the inverter to the residential load despite the power demand from the generator. This increases system efficiency since no power flow changes take place in the transmission system. Another key aspect of the paper is the novelty of the speed controller. The speed controller concept for PMLGs operates similarly to a complex conjugate control system but with less requirements for measurements. The implementation of the speed controller in wave energy devices is a future target of this research. Based on the simulation results presented in this paper off-grid loads can be supplied by a WEC farm with the above mentioned electrical configuration. However, since waves are not always present there is always the need of a grid-forming inverter to keep system frequency constant and provide autonomy to the residential load.

Acknowledgements

The authors would like to acknowledge the support of the Newton Fund and EPSRC in funding the work within this paper (EP/M020231/1) and also the Programme of Introducing Talents of Discipline to Universities (“111 Programme”) Grant No.: B14028.

References

1 Kiprakis, A.E., Nambiar, A.J., Forehand, D., Wallace, A.R.: ‘Modelling arrays of wave energy converters connected to weak rural electricity networks’, in ‘2009 International Conference on

Sustainable Power Generation and Supply' (IEEE, 2009), pp. 1–7

2 Tedeschi, E., Santos-Mugica, M.: 'Modeling and Control of a Wave Energy Farm Including Energy Storage for Power Quality Enhancement: the Bimep Case Study'*IEEE Trans. Power Syst.*, 2014, **29**, (3), pp. 1489–1497.

3 Zanxiang Nie, Xi Xiao, Qing Kang, Aggarwal, R., Huiming Zhang, Weijia Yuan: 'SMES-Battery Energy Storage System for Conditioning Outputs From Direct Drive Linear Wave Energy Converters'*IEEE Trans. Appl. Supercond.*, 2013, **23**, (3), p. 5000705.

4 Di Noia, L.P., Del Pizzo, A., Brando, G., Dannier, A., Pisani, C.: 'Grid connection of wave energy converter in heaving mode operation by supercapacitor storage technology'*IET Renew. Power Gener.*, 2016, **10**, (1), pp. 88–97.

5 Gunn, K., Stock-Williams, C.: 'Quantifying the global wave power resource'*Renew. Energy*, 2012, **44**, pp. 296–304.

6 Mørk, G., Barstow, S., Kabuth, A., Pontes, M.T.: 'Assessing the Global Wave Energy Potential', in '29th International Conference on Ocean, Offshore and Arctic Engineering: Volume 3' (ASME, 2010), pp. 447–454

7 Titah-Benbouzid, H., Benbouzid, M.: 'Ocean wave energy extraction: Up-to-date technologies review and evaluation', in 'Proceedings of the 2014 IEEE PEAC' (2014), pp. 338–342

8 Forehand, D.I.M., Kiprakis, A.E., Nambiar, A.J., Wallace, A.R.: 'A Fully Coupled Wave-to-Wire Model of an Array of Wave Energy Converters'*IEEE Trans. Sustain. Energy*, 2016, **7**, (1), pp. 118–128.

9 Vining, A.J., Muetze, A.: 'Linear Generators for Direct-Drive Ocean Wave Energy Conversion'2007, pp. 798–804.

10 Feng Wu, Xiao-Ping Zhang, Ping Ju, Sterling, M.: 'Modeling and Control of AWS-Based Wave Energy Conversion System Integrated Into Power Grid'*IEEE Trans. Power Syst.*, 2008, **23**, (3), pp. 1196–1204.

11 Spooner, E., Tavner, P., Mueller, M.A., Brooking, P.R.M., Baker, N.J.: 'Vernier hybrid machines for compact drive applications', in 'Second IEE International Conference on Power Electronics, Machines and Drives' (IEE, 2004), pp. 452–457

12 Brooking, P.R.M., Mueller, M.A.: 'Power conditioning of the output from a linear vernier hybrid permanent magnet generator for use in direct drive wave energy converters'*IEE Proc. - Gener. Transm. Distrib.*, 2005, **152**, (5), pp. 673–681.

13 Ringwood, J. V, Bacelli, G., Fusco, F.: 'Energy-Maximizing Control of Wave-Energy Converters: The Development of Control System Technology to Optimize Their Operation'*IEEE Control Syst.*, 2014, **34**, (5), pp. 30–55.

14 Shek, J.K.H., Macpherson, D.E., Mueller, M.A., Xiang, J.: 'Reaction force control of a linear electrical generator for direct drive wave energy conversion'*IET Renew. Power Gener.*, 2007, **1**, (1), pp. 17–24.

15 Rahm, M., Boström, C., Svensson, O., *et al.*: 'Offshore underwater substation for wave energy converter arrays'*IET Renew. Power Gener.*, 2010, **4**, (6), pp. 602–612.

16 Polinder, H., Slootweg, J.G., Hoeijmakers, M.J., Compter, J.C.: 'Modeling of a linear pm machine including magnetic saturation and end effects: maximum force-to-current ratio'*IEEE Trans. Ind. Appl.*, 2003, **39**, (6), pp. 1681–1688.

17 Annuar, A.Z., Macpherson, D.E., Forehand, D.I.M., Mueller, M.A.: 'Optimum power control for arrays of direct drive wave energy converters', in '6th IET International Conference on Power Electronics, Machines and Drives (PEMD 2012)' (IET, 2012), pp. 1–6

18 Li, B., Macpherson, D.E., Shek, J.K.H.: 'Direct drive wave energy converter control in irregular waves', in 'IET Conference on Renewable Power Generation (RPG 2011)' (IET, 2011), pp. 1–6

19 Wu, B., Lang, Y., Zargari, N., Kouro, S.: 'Variable-speed wind energy systems with synchronous generators', in 'Power Conversion and Control of Wind Energy Systems' (John Wiley & Sons, Inc., 2011), pp. 275–316

20 Gan, L.K., Shek, J.K.H., Mueller, M.A.: 'Modelling and experimentation of grid-forming inverters for standalone hybrid wind-battery systems', in '2015 International Conference on Renewable Energy

Research and Applications (ICRERA)' (IEEE, 2015), pp. 449–454

21 Macpherson, D.E., Mueller, M.A., Shek, J.K.H.: 'Power conversion for wave energy applications', in '5th IET International Conference on Power Electronics, Machines and Drives (PEMD 2010)' (Institution of Engineering and Technology, 2010), pp. 1–6

22 Salter, S.H., Taylor, J.R.M., Caldwell, N.J.: 'Power conversion mechanisms for wave energy'*Proc. I MECH E Part M*, 2002, **216**, (1), pp. 1–27.

23 'MAXWELL TECHNOLOGIES', http://www.maxwell.com/, accessed November 2016

24 Collin, A.J., Tsagarakis, G., Kiprakis, A.E., McLaughlin, S.: 'Development of Low-Voltage Load Models for the Residential Load Sector'*IEEE Trans. Power Syst.*, 2014, **29**, (5), pp. 2180–2188.